Contents lists available at ScienceDirect

Engineering Analysis with Boundary Elements

Stochastic modelling of nanofluids using the fast Boundary-Domain Integral Method

J. Ravnik [a,*], A. Šušnjara [b], J. Tibaut [a], D. Poljak [b], M. Cvetković [b]

[a] *Faculty of Mechanical Engineering, University of Maribor, Smetanova ulica 17, Maribor SI-2000, Slovenia*
[b] *Faculty of Electrical Engineering, Mechanical Engineering and Naval Architecture, University of Split, Croatia*

A R T I C L E   I N F O

A B S T R A C T

In this paper, we couple a numerical method aimed at simulation of flow and heat transfer of nanofluids with stochastic modelling of input and material parameters. In order to simulate nanofluids, an in-house numerical method was developed, based on the solution of 3D velocity–vorticity formulation of Navier–Stokes equations. A fast Boundary-Domain Integral Method has been employed to solve the governing equations and set up the deterministic flow and heat transfer solver. The developed algorithm is used to simulate natural convection of a nanofluid in a closed cavity. The uncertainty present in the input parameters is propagated to the output of interest via the Stochastic Collocation Method. The stochastic mean, variance, and higher-order moments of the output values are presented. The non-intrusive nature of the Stochastic Collocation Method facilitates the previously validated deterministic code to remain unchanged. The stochastic analysis reveals that the uncertainty of input parameters influences the output results most in the areas where high flow field gradients appear.

1. Introduction

Modelling and simulation [1] of natural phenomena and technical devices has become a standard tool for researchers and engineers in their quest to understand the phenomena and processes and optimise their solutions and designs. The first step in the modelling process is the identification of processes, variables and parameters. A mathematical-physical model of the processes is set up, which connects the processes with variables and parameters. In many cases, the mathematical-physical model is very well known, for example, in fluid dynamics and heat transfer, the Navier–Stokes equations [2] are known to describe the underlying processes adequately. Models are based on several parameters. These may come from design considerations or represent material properties. In virtually all cases, the parameters are known only with a certain degree of accuracy. Furthermore, the parameters may be temperature or pressure dependent, which, when not taken into account, is another source of uncertainty.

The usual practice in the numerical simulation of nanofluids is to use average values of input parameters, thus leading to merely a rough representation of reality. However, the uncertainty present in input parameters can be quantified by using the statistical/stochastic tools [3–5] and propagated to the output value of interest via a suitable uncertainty propagation method. Sensitivity and uncertainty analysis has

been successfully employed to study key input parameters influencing a wide variety of systems [6]. Vu-Bac et al. [7] have developed a software framework for probabilistic sensitivity analysis for computationally expensive models to avoid the high computational demand of the traditional Monte Carlo method [8]. Xiu and Karniadakis [9] and Thapa et al. [10] proposed modelling uncertainty in flow simulations via generalised polynomial chaos. They showed that the generalised polynomial chaos method promises a substantial increase to the convergence rate compared with the Monte Carlo method. Mathelin et al. [11] compared two stochastic approaches to uncertainty quantification in flow simulations: polynomial chaos and stochastic collocation, showing the advantage of the stochastic collocation. In this work, the Stochastic Collocation Method (SCM) is used [12].

Successful applications of the SCM have been reported in different areas, e.g. stochastic analysis of convective heat transfer [13] and uncertainty quantification in computational fluid dynamics [14], electrostatic micromechanical systems [15], numerical simulation of a reverberation chamber [16], uncertainty quantification of specific absorption rate in numerical dosimetry [17], etc. The SCM has many variants, depending on the problem to be solved and the number of the input parameters to be modelled as random variables/processes [12]. The main advantage of the SCM is its nonintrusive nature which allows the use of unchanged deterministic codes that were validated previously. However,

---

* Corresponding author.
E-mail addresses: jure.ravnik@um.si (J. Ravnik), ansusnja@fesb.hr (A. Šušnjara), jan.tibaut@um.si (J. Tibaut), dpoljak@fesb.hr (D. Poljak), mcvetkov@fesb.hr (M. Cvetković).

unlike traditional Monte Carlo methods, the choice of sampling points is not random. Instead, the points are selected according to the quadrature or cubature rules, chosen carefully in order to compute the integrals of stochastic moments as accurately as possible [12]. The SCM framework is used in this work with the aim to compute the stochastic mean and variance of the output values. Additionally, a sensitivity analysis based on a *one-at-a-time* approach is carried out to identify the relative impact of different input parameters.

In order to apply the stochastic modelling of input parameters, we propose to use the fast Boundary-Domain Integral Method (BDIM) to perform deterministic simulations. The BDIM was proposed by Škerget et al. [18] for the solution of the Navier–Stokes equations in velocity–vorticity form. As the governing equations are unsteady, non-linear and inhomogeneous, a straightforward boundary only integral representation is not possible. In its original form, BDIM uses a domain mesh to evaluate domain integrals in the boundary-domain integral representation. Use of different Green's functions is possible, such as the fundamental solution of the diffusion operator, or the convection–diffusion operator. Since all are non-local, the resulting domain integral matrix is fully populated and unsymmetrical. The CPU time and memory storage requirements of the BDIM scale as $\mathcal{O}(n^2)$, where n is the number of all nodes in the boundary and domain meshes. This scaling limits the applicability of the method severely, as it can only be applied to small problems due to its huge computational demands.

Several attempts have already been made in order to mitigate the main drawback of BDIM and reduce the scaling of computational demands to a more manageable $\mathcal{O}(n \log n)$. Either boundary or domain matrices coming from the discretisation of the integral equations can be approximated using a wide variety of approaches, known by a joint name: *fast* methods. The Fast Multipole Method (FMM) [19,20], the Adaptive Cross Approximation (ACA) [21–25] and wavelet transform [26–28] are among the more popular approaches. Domain integrals may be avoided by transforming them into boundary integrals either by means of approximation within the domain (dual reciprocity method, [29,30]), or by using the radial integration method, [31,32]. Another popular approach is based on domain decomposition [33–35].

The solution of Navier–Stokes equations proposed in this paper uses BDIM accelerated by a combination of two fast approaches: the ACA and domain decomposition. ACA is used to approximate integral matrices stemming from the kinematics equations and domain decomposition is used for the vorticity and energy transport equations.

The deterministic fast BDIM algorithm was coupled with a stochastic method in this paper to assess the influence of input parameters in the case of flow and heat transfer of nanofluids [36]. A nanofluid is a stable suspension of a base fluid and nanometre-sized particles. Usually, the base fluid has poor thermal characteristics (e.g. water, glycol). Thus, the introduction of particles with good thermal properties (such as metal oxides) improves the thermal properties of the suspension significantly. Since particles are nanometre-sized, the suspensions remain stable for a long period of time due to Brownian motion and natural convection. Such suspensions are named nanofluids. In recent years, research into nanofluids has intensified in the fields of Material Characterisation [37,38], Engineering Application [39] and Simulation [40–42]. In this work, we employ the homogeneous effective properties nanofluid model [40] and use the appropriate Navier–Stokes equations in velocity–vorticity formulation. We are interested in the input parameter influence on the results for a specific flow and heat transfer case. However, stochastic methods can also be used to estimate effective parameters of nanofluids, as proposed by Kaminski and Ossowski [43].

The paper is organised as follows: first, the governing equations are presented, followed by the description of the fast BDIM method. The stochastic modelling approach is presented in Section 4. Section 5 presents the nanofluid problem under consideration, and is followed by the Results section. The summary of the paper is given in the last section.

2. Governing equations

We suppose that the nanofluid is a dilute suspension of uniformly dispersed nanometre-sized particles in the base fluid. The nanofluid behaves as an incompressible Newtonian fluid, and we assume that the nanoparticles and the fluid are in thermal equilibrium. Furthermore, we assume the no-slip boundary condition between the particles and the fluid. Within these approximations, the nanofluid can be modelled as a new fluid with newly defined effective properties. These properties are: thermal conductivity k_{nf}, density ρ_{nf}, viscosity ν_{nf}, heat capacitance c_{nf} and thermal expansion coefficient β_{nf}. From here on, we denote nanofluid properties with the subscript nf, the solid particle properties with s, and pure base fluid properties with the subscript f. The effective nanofluid properties are all assumed constant throughout the flow domain, although, they do depend on the nanoparticle concentration. The assumption of constant properties is justifiable, due to the fact that thermal properties of base fluid (water) do not depend strongly on temperature, and, at the same time, the Stokes number of nanoparticles is very small, and the influence of Brownian motion on nanoparticles is substantial, thus, the assumption of uniform distribution of nanoparticles, which leads to constant nanofluid properties, is justified. Finally, we assume the flow to be laminar and steady, since we are interested in steady state improvement of heat transfer due to the presence of nanoparticles.

The flow of nanofluid is governed by the Navier–Stokes equations coupled with the energy transfer equation. They should be solved for the unknown velocity, pressure and temperature fields. In this paper, we employ the velocity–vorticity formulation of Navier–Stokes equations, where the pressure is replaced by vorticity in the governing equations. Vorticity is defined at the curl of the velocity field. We propose to solve the problem in a non-dimensional manner by introducing the following characteristic parameters: temperature T_0, temperature difference ΔT, length scale L and $g_0 = 9.81 \text{ m/s}^2$. We will study the development of natural convection, thus, a natural choice for characteristic velocity, which would be defined from the flow rate, does not exist. We chose the characteristic velocity to be $v_0 = k_f/(\rho c)_f L$. This choice leads to the following definition of the Reynolds number $Re = 1/Pr$, where Pr is the pure fluid Prandtl number, $Pr = \nu_f (\rho c)_f / k_f$. The nondimensional flow field vectors are defined as follows, the velocity field $\vec{v} = \vec{v}^\star/v_0$, the position vector $\vec{r} = \vec{r}^\star/L$, the vorticity field $\vec{\omega} = L\vec{\omega}^\star/v_0$, temperature field $\theta = (T^\star - T_0)/\Delta T$ and $\vec{g} = \vec{g}^\star/g_0$. Starred parameters denote dimensional values. Within this nondimensional setting, one can derive the nondimensional steady velocity–vorticity formulation of Navier–Stokes equations. A system of three second order partial differential equations is obtained, namely, the kinematics equation, the vorticity transport equation and the energy equation [44]:

$$\nabla^2 \vec{v} + \vec{\nabla} \times \vec{\omega} = 0, \tag{1}$$

$$(\vec{v} \cdot \vec{\nabla})\vec{\omega} = (\vec{\omega} \cdot \vec{\nabla})\vec{v} + Pr \frac{\nu_{nf}}{\nu_f} \frac{\rho_f}{\rho_{nf}} \nabla^2 \vec{\omega} - PrRa \frac{\beta_{nf}}{\beta_f} \vec{\nabla} \times \theta \vec{g}, \tag{2}$$

$$(\vec{v} \cdot \vec{\nabla})\theta = \frac{k_{nf}}{k_f} \frac{(\rho c)_f}{(\rho c)_{nf}} \nabla^2 \theta. \tag{3}$$

Apart from the ratios between the pure fluid and nanofluid properties, the problem is described uniquely by specifying Rayleigh and Prandtl number values for the pure fluid. The Rayleigh number is defined as $Ra = g_0 \beta_f \Delta T L^3 \rho_f (\rho c_p)_f / (\nu_f k_f)$. Furthermore, either Dirichlet or Neumann velocity, vorticity and temperature boundary conditions must be known. We assume that the velocity and temperature boundary conditions are known, while we calculate the vorticity boundary conditions, which are need for the solution of Eq. (2), within the nonlinear iteration loop. Pressure is not a part of the velocity–vorticity formulation of Navier–Stokes equations. It can be calculated in a post-processing step from the known velocity and vorticity fields.

The nanofluid density, heat capacity and thermal expansion coefficient are defined using the mixing rule [45] based on the nanoparticle

volume fraction φ as: $\rho_{nf} = (1 - \varphi)\rho_f + \varphi\rho_s$, $(\rho c)_{nf} = (1 - \varphi)(\rho c)_f + \varphi(\rho c)_s$ and $(\rho\beta)_{nf} = (1 - \varphi)(\rho\beta)_f + \varphi(\rho\beta)_s$.

A model for effective viscosity of a dilute suspension of small rigid spherical particles in water was developed by Brinkman [46]: $\nu_{nf} = \nu_f/(1 - \varphi)^{2.5}$. The Maxwell-Garnett formula [47,48] is available for estimation of the effective thermal conductivity of a nanofluid

$$k_{nf} = k_f \frac{k_s + 2k_f - 2\varphi(k_f - k_s)}{k_s + 2k_f + \varphi(k_f - k_s)}. \tag{4}$$

3. The fast Boundary-Domain Integral Method

Our aim is to solve a set of three nonlinear partial differential equations (1)–(3) in a deterministic way by specifying the nanofluid properties and Rayleigh and Prandtl numbers. The BDIM uses a fundamental solution of the diffusion operator to derive integral expressions for the set of governing equations. The integral statements are discretised on a computational grid, and this leads to fully populated systems of linear equations. Fully populated matrices may be approximated using one of the fast methods. In this work, we use adaptive cross approximation and transformations of the matrices in $\mathcal{H}$ matrix format. Since the set of governing equations is nonlinear, an iteration loop is set up, which uses under-relaxation to reach convergence.

Let Ω denote the fluid domain, with a position vector $\vec{r} \in (\mathbb{R})^3$, and let Γ be its boundary and $\vec{\xi}$ a point in the domain or on the boundary. Starting from Green's theorems, it is possible to derive the singular boundary-domain integral representation of the governing equations. We make use of the fundamental solution of the Laplace equation $u^\star(\vec{\xi}, \vec{r}) = 1/4\pi|\vec{\xi} - \vec{r}|$.

Wu and Thompson [49] and Škerget et al. [50] derived the following integral form of the kinematics equation (1):

$$c(\vec{\xi})\vec{v}(\vec{\xi}) + \int_\Gamma \vec{v}(\vec{n} \cdot \vec{\nabla} u^\star)d\Gamma = \int_\Gamma \vec{v} \times (\vec{n} \times \vec{\nabla} u^\star)d\Gamma + \int_\Omega (\vec{\omega} \times \vec{\nabla} u^\star)d\Omega, \tag{5}$$

Ravnik et al. [44] derived the integral forms of the vorticity transport equation (2) and the energy equation (3) as follows:

$$c(\vec{\xi})\omega_j(\vec{\xi}) + \int_\Gamma \omega_j \vec{\nabla} u^* \cdot \vec{n} d\Gamma = \int_\Gamma u^* q_j d\Gamma$$
$$+ \frac{1}{Pr}\frac{\nu_f}{\nu_{nf}}\frac{\rho_{nf}}{\rho_f}\left(\int_\Gamma \vec{n} \cdot \{u^*(\vec{v}\omega_j - \vec{\omega}v_j)\}d\Gamma - \int_\Omega (\vec{v}\omega_j - \vec{\omega}v_j) \cdot \vec{\nabla} u^* d\Omega\right)$$
$$- Ra\frac{\beta_{nf}}{\beta_f}\frac{\nu_f}{\nu_{nf}}\frac{\rho_{nf}}{\rho_f}\int_\Gamma (u^\star\theta\vec{g} \times \vec{n})_j d\Gamma - Ra\frac{\beta_{nf}}{\beta_f}\frac{\nu_f}{\nu_{nf}}\frac{\rho_{nf}}{\rho_f}\int_\Omega (\theta\vec{\nabla} \times u^\star\vec{g})_j d\Omega, \tag{6}$$

$$c(\vec{\xi})\theta(\vec{\xi}) + \int_\Gamma \theta\vec{\nabla} u^* \cdot \vec{n} d\Gamma = \int_\Gamma u^*\theta_q d\Gamma$$
$$+ \frac{k_f}{k_{nf}}\frac{(\rho c_p)_{nf}}{(\rho c_p)_f}\left(\int_\Gamma \vec{n} \cdot \{u^*(\vec{v}\theta)\}d\Gamma - \int_\Omega (\vec{v}\theta) \cdot \vec{\nabla} u^* d\Omega\right). \tag{7}$$

Here, θ_q is the temperature flux, i.e. $\theta_q = \vec{n} \cdot \vec{\nabla}\theta$ and q_j is the jth component of vorticity flux. $\vec{n}$ is a vector normal to the boundary, pointing out of the domain. $c(\vec{\xi})$ is the geometric factor defined as $c(\vec{\xi}) = \alpha/4\pi$. When $\vec{\xi}$ is at the boundary, α is the inner angle of the boundary with the origin at $\vec{\xi}$. When the boundary is straight, $c = 1/2$, when $\vec{\xi}$ is in the domain, $c = 1$.

The boundary-domain integral representations of the governing equations (5)–(7) all feature boundary as well as domain integrals. When non-fast BDIM is used, we prepare a computational grid in the domain and at the boundary and, place the source point $\vec{\xi}$ in all boundary nodes. This leads to fully populated systems of linear equations, which, due to the presence of domain terms, scale as the number of domain nodes squared. The fully populated system limits the applicability of BDIM severely, since it requires large computational resources. In this paper, we want to couple this deterministic algorithm with stochastic estimation of the influence of input parameters. This requires many runs of the

deterministic algorithm (around twenty thousand runs were performed to produce the results presented in this paper). Thus, we introduced two *fast* techniques to lower the required computational resources: the $\mathcal{H}$ matrix structure and ACA approximation for the kinematics equation (5), and a domain decomposition approach for the vorticity (6) and temperature (7) equations.

We employ hexahedrons to set up the domain mesh and their faces for the boundary mesh. At the boundary and in the domain we employ continuous quadratic interpolation for function and discontinuous linear interpolation for flux using shape functions φ, ϕ and Φ:

$$u = \sum_{i=1}^{9} \varphi_i u_i, \qquad q = \sum_{i=1}^{4} \phi_i q_i, \qquad u = \sum_{i=1}^{27} \Phi_i u_i, \tag{8}$$

where u represents the field functions and q their flux. The flux interpolation nodes are located inside of the boundary elements so the element normal is well defined in each flux node. Using these interpolations we are able to write discrete counterparts of the governing equations.

The complete algorithm can be summarised as follows. Firstly, we employ the $\mathcal{H}$ matrix structure and ACA accelerated solution of the kinematics equation (5) to determine vorticity values at the boundary. Next, we use the domain decomposition approach to solve the velocity field using (5), temperature field using (7) and, vorticity field using (6). For the solution of (6) we make use of boundary vorticity values obtained in the first step of the algorithm. Since the problem is non-linear, we repeat these steps until convergence for all field functions is reached. Convergence criteria are based on the relative difference between field functions in the current and the previous iteration. It was set to 10^{-5}. To mitigate the nonlinear nature of the problem, we employed under-relaxation for the energy equation (10%) and the vorticity equation (1%). Both fast approaches are presented in the following subsections.

3.1. ACA – $\mathcal{H}$ matrix approach

We use the ACA – $\mathcal{H}$ matrix approach to decrease the computational demands of the solution of the kinematics equation (5) for the unknown boundary vorticity values. We base our method on a full domain computational grid, since the integral form of the equation features both boundary and domain integrals. Nowadays, the meshing of the domain with modern meshing algorithms is no longer a challenge, and cannot be regarded as a disadvantage of the method. However, full matrices, which are produced during the discretisation, do indeed present a problem. In the case of the kinematics equations, we place source points only into the boundary nodes. We encounter two types of matrices: Boundary × boundary and boundary × domain. In order to use ACA to produce low-rank approximations of the matrices, we first transform the matrices into $\mathcal{H}$ matrix format [51]. Hierarchical decomposition of the domain can be achieved using a top-down approach [25] or a bottom-up approach [23]. In this work, we employ the bottom-up approach. The decomposition is done twice, firstly for the boundary, where boundary nodes are grouped into boundary clusters, and secondly for the domain, where domain nodes are grouped into domain clusters (Fig. 1). An admissibility criterion is used, based on the size of the clusters and distance between the clusters, to decide which cluster pair can be approximated by ACA and which cannot. An illustration of admissible parts of a matrix is presented in Fig. 1. Additional information on the implementation of the approach is given in Ravnik and Tibuat [25] and Tibaut and Ravnik [24].

3.2. Domain decomposition approach

The domain decomposition approach is used for equations (5), (7) and (6) to solve the velocity, temperature and vorticity fields. Instead of applying BDIM on the whole mesh, we apply BDIM for each mesh cell individually. As boundary conditions between mesh cells are unknown, we introduce continuity of functions and preservation of flux between cells as additional constraints. This approach was proposed by
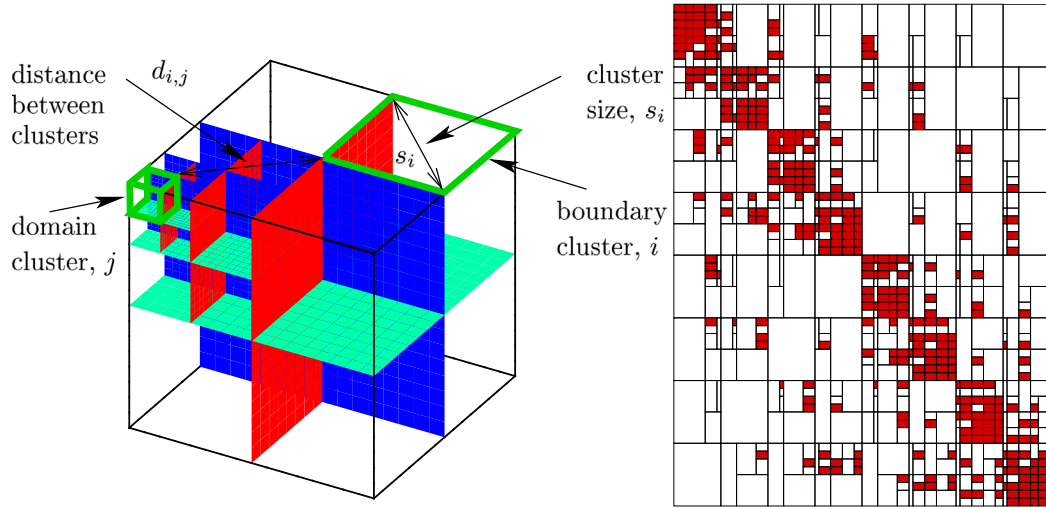
Fig. 1. Hierarchical division of a cubic domain is shown in the left panel. Boundary and domain clusters are presented, together with the definition of the distance between clusters and the size of clusters. In the right panel, a corresponding boundary-domain matrix structure for an 17^3 nodes mesh is shown. Inadmissible parts are shown in red. (For interpretation of the references to colour in this figure legend, the reader is referred to the web version of this article.)

Ramšak and Škerget [52] for stream function-vorticity formulation in 2D, and extended to the velocity–vorticity formulation in 3D by Ravnik et al. [53]. Since subdomains share nodes, and since we place collocation points in every function and flux node we end up with more equations than unknowns. The resulting over-determined sparse system of linear equations is solved by a least-squares-based solver. The system is sparse because subdomains are mesh cells and each equations only connects function and flux with neighbouring subdomains.

4. Stochastic modelling

In order to assess the uncertainty present in material parameters and design parameters, we will employ the Stochastic Collocation Method (SCM) to propagate the uncertainty to simulation results, which are of engineering importance.

4.1. Sensitivity moments

The fundamental principle of the SCM lies in the polynomial approximation of the considered output over the multi-dimensional input stochastic space [12]:

$$Y(\mathbf{X}) = \sum_{i=1}^{N} L_i(\mathbf{X}) \cdot Y^{(i)} \tag{9}$$

where $L_i(\mathbf{X})$ is the basis function, $Y^{(i)}$ is the output realisation for the ith input point $\mathbf{X}^{(i)}$ and N is the total number of deterministic simulations. The random input variables are organised in a vector $\mathbf{X}^{(i)} = [x_1^{(i)}, \dots x_d^{(i)}]$ where d is the total number of input random variables (RV). The basis functions may be of Lagrange type [14], wavelet basis [54] or piecewise constant [15] while the choice of the collocation points may follow different quadrature [14] and cubature rules [55].

Throughout this work a Lagrange type of basis functions is adopted. Hence, for the univariate case, i.e. $d = 1$ and $\mathbf{X}^{(i)} = [x_1^{(i)}]$ and a total of m_k collocation points in the kth dimension the Lagrange basis function is given as:

$$L_i(x_k) = l_i(x_k) = \prod_{j=0, j \neq i}^{k} \frac{x_k - x_k^{(j)}}{x_k^{(i)} - x_k^{(j)}}, \qquad i = 1, \dots, m_k \tag{10}$$

with the property $l_i(x_j) = \delta_{ij}$, where δ_{ij} denotes the Kronecker symbol. In order to answer the question about collocation points' selection, it is useful firstly to recall the definitions of stochastic moments. The stochastic mean μ, standard deviation σ, and variance σ^2 are defined as follows:

$$\mu(Y(\mathbf{X})) = \int_{\Gamma} Y(\mathbf{X}) p(\mathbf{X}) d\mathbf{X}, \tag{11}$$

$$\sigma^2(Y(\mathbf{X})) = \int_{\Gamma} (Y(\mathbf{X}) - \mu(Y(\mathbf{X})))^2 p(\mathbf{X}) d\mathbf{X} = \int_{\Gamma} (Y(\mathbf{X}))^2 p(\mathbf{X}) d\mathbf{X} - (\mu(Y(\mathbf{X})))^2, \tag{12}$$

where $p(\mathbf{X})$ is the joint probability density function:

$$p(\mathbf{X}) = \prod_{k=1}^{d} p(x_k) \tag{13}$$

and Γ is the support space of random input variables. Using the polynomial expansion (9) we can approximate the expression for mean (11) and variance (12) as

$$\mu(Y(\mathbf{X})) \approx \sum_{i=1}^{N} Y^{(i)} \int_{\Gamma} L_i(\mathbf{X}) p(\mathbf{X}) d\mathbf{X} \tag{14}$$

and

$$\sigma^2(Y(\mathbf{X})) \approx \sum_{i=1}^{N} \left(Y^{(i)}\right)^2 \int_{\Gamma} L_i(\mathbf{X}) p(\mathbf{X}) d\mathbf{X} - (\mu(Y(\mathbf{X})))^2 \tag{15}$$

Since the basis functions $L_i(\mathbf{X})$ and the joint pdf $p(\mathbf{X})$ are known, the integral over the space Γ can be precomputed and its value is called the weight w_i:

$$w_i = \int_{\Gamma} L_i(\mathbf{X}) p(\mathbf{X}) d\mathbf{X}. \tag{16}$$

Consequently, the stochastic moments mean, variance, skewness and kurtosis can be expressed in a very simple form, [12], as

$$\mu \approx \sum_{i=1}^{N} Y^{(i)} w_i, \qquad \sigma^2 \approx \sum_{i=1}^{N} \left(Y^{(i)}\right)^2 w_i - \mu^2, \tag{17}$$

$$skew \approx \frac{1}{\sigma^3} \left(\sum_{i=1}^{N} \left(Y^{(i)}\right)^3 w_i - 3\mu\sigma^2 - \mu^3 \right), \tag{18}$$

$$kurt \approx \frac{1}{\sigma^4} \left(\sum_{i=1}^{N} \left(Y^{(i)}\right)^4 w_i - 4\mu\sigma^3 \cdot skew - 6\mu^2\sigma^2 - \mu^4 \right). \tag{19}$$

Due to interpolative nature of the SCM, the accuracy of mean and variance is expected to be higher than the accuracy of higher-order moments.

In the case when the stochastic dimension is equal to $d = 1$, the collocation points' selection is straightforward, as it depends on the choice of quadrature rule. The optimal choice is Gauss quadrature [12]. Depending on the pdf of the input random variables, one can choose between different Gauss quadrature rules, e.g. Gauss–Hermite, Gauss–Legendre or Gauss–Jacobi for variables with normal, uniform or beta distributions, respectively.

The real challenge, however, is a numerical computation of multi-dimensional integral for $d > 1$, especially for $d \gg 1$. The most natural approach to multi-dimensional integration is the tensor product of 1-dimensional quadrature rules which leads to relatively simple generalisation of integration properties from 1-dimensional to d-dimensional case [12]. The multi-dimensional integral for the calculation of weights (16) is, thus, given as:

$$w_i = \int_{\Gamma_1} l_i(\mathbf{X_1}) p(\mathbf{X_1}) d\mathbf{X_1} \cdot \int_{\Gamma_2} l_i(\mathbf{X_2}) p(\mathbf{X_2}) d\mathbf{X_2} \cdot \ldots \cdot \int_{\Gamma_d} l_i(\mathbf{X_d}) p(\mathbf{X_d}) d\mathbf{X_d}.$$

(20)

The total number of simulation points is $\prod_{k=1}^{d} m_k$. The basis function $L_i(\mathbf{X})$ is given as the tensor product of 1-dimensional Lagrange basis function in each dimension:

$$L_i(\xi) = l(\xi_1^{(i)}) \otimes l(\xi_2^{(i)}) \otimes \ldots \otimes l(\xi_d^{(i)})$$

(21)

In most of the applications, the number of collocation points in each dimension is equal, i.e. $\forall k \Rightarrow m_k = m$, thus the total number of simulations is m^d. Obviously, the number of simulation points grows exponentially with the number of input random variables, therefore the tensor product is used mostly at lower dimensions. The generally accepted limitation is $d \leq 5$ [12]. For higher dimensions $d \gg 1$, different variants of sparse grid algorithms are proposed, which reduce the total number of points w.r.t. tensor product rules tremendously [12]. In order establish the appropriate value for the number of collocation points m_k, we increase m_k up to the point where the results converge to a stable common value.

4.2. Sensitivity analysis

The definition for the sensitivity analysis adopted in this work, is the study of how the uncertainty in the output of a mathematical model or system (numerical or otherwise) can be apportioned to different sources of uncertainty in its inputs [56]. The ideal approach would be to run both uncertainty quantification and sensitivity analysis in the same stochastic framework, usually uncertainty quantification preceding the sensitivity analysis, thus minimising the computational burden as much as possible. Within the presented stochastic framework the sensitivity is measured by monitoring the change in the variance of the output after computing the variance for d univariate cases. Thus, the impact factor of each input parameter is given by the following formula:

$$I_i = \frac{\sigma_i^2(Y)}{\sigma^2(Y)}$$

(22)

where $\sigma^2(Y)$ is the total variance of d-dimensional case, and $\sigma_i^2(Y)$ is the variance of the ith one-dimensional case. This approach may be defined as a *one-at-a-time* (OAT) approach. Although it cannot detect the presence of interactions between input variables, it is still a computationally inexpensive way of identifying the relative impact of the input variables.

5. Nanofluid flow problem

We apply the methods developed in this paper by simulating the flow and heat transfer of water-based nanofluid seeded with Al_2O_3 nanoparticles. The thermophysical properties of water and solid Al_2O_3 nanoparticles were taken from Oztop and Abu-Nada [57], and are listed in Table 1.

We study the development of natural convection in a differentially heated cubic cavity. We consider six cases combining two nanoparticle volume fractions ($\varphi = 2.5\%$ and $\varphi = 5\%$) and three Rayleigh number values ($Ra = 10^3$, $Ra = 10^4$ and $Ra = 10^5$).

Table 1
Thermophysical properties of pure fluids and solid nanoparticles [57]. Water viscosity is $\nu = 0.912 \, \text{mm}^2/\text{s}$.

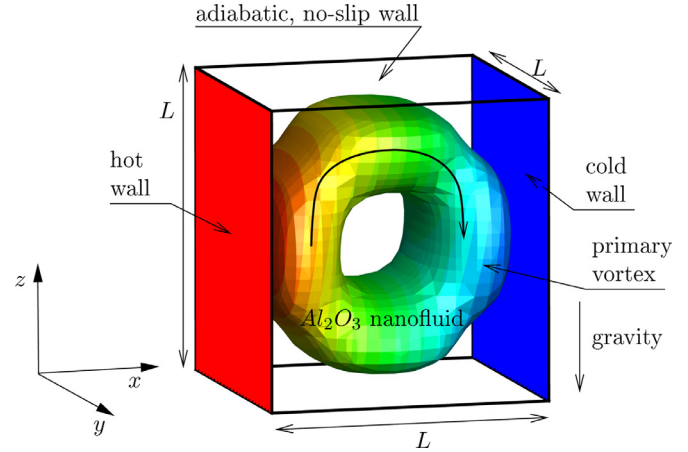|	c_p [J/kg K]	ρ [kg/m^3]	k [W/mK]	β [$\cdot 10^{-5}$ K^{-1}]
Water	4179	997.1	0.613	21
Al_2O_3	765	3970	40	0.85

Fig. 2. Boundary conditions for the natural convection in a cubic cavity test case. All six sides of the cavity have a no-slip boundary condition applied. Dirichlet constant temperature boundary conditions are prescribed on the hot and cold walls. Neumann zero heat flux boundary condition is applied on the other four walls. Primary vortex and its orientation are also shown. Temperature contours are shown on the velocity magnitude isosurface for the $Ra = 10^3$ case.

The boundary conditions are as follows: Two opposite vertical walls are heated and/or cooled to a constant temperature. All the other walls are adiabatic. In terms of the velocity field, all walls have a no-slip boundary condition applied. Vorticity boundary conditions are calculated during the algorithm, as described above. Initially, the flow velocity is zero, but during the simulation, a steady laminar flow develops, which features a large clockwise rotating vortex carrying the nanofluid up the hot wall and down the cold wall. We analyse the flow structure and heat transfer in steady state. The flow domain and the boundary conditions are shown in Fig. 2.

The nanofluid flow is a function of the domain geometry, boundary conditions and effective properties. For engineering practice, the wall heat flux is an important parameter, which reveals the effectiveness of a nanofluid as compared to other fluids. The heat flux $\dot{Q}$ can be written using the pure fluid thermal conductivity, characteristic flow scales and a nondimensional Nusselt number, i.e. $\dot{Q} = k_f L \Delta T \cdot Nu$. The Nusselt number, Nu, is defined as the integral of the temperature flux at a wall, i.e. $Nu = \frac{k_{nf}}{k_f} \int_{\Gamma} \vec{\nabla} T \cdot \vec{d\Gamma}$, where $\vec{\Gamma}$ is the wall. Variation of heat flux over the surface of the wall is expressed using the local Nusselt number: $Nu_l = k_{nf}/k_f \vec{\nabla} T \cdot \vec{\Gamma}/|\vec{\Gamma}|$.

Since a very large number of simulations is foreseen, (around 20,000), we had to be careful to choose a computational mesh, which generates results fast enough so that 20,000 simulations are feasible, and, at the same time, is dense enough to produce mesh-independent results. In order to determine the appropriate mesh density, we meshed the domain with hexahedral elements having 17^3, 25^3 and 41^3 nodes, and ran the simulations with $\varphi = 5\%$ and $Ra = 10^3$. We compared the heat flux through the hot wall, and found the values expressed as Nusselt number to be 1.1857, 1.1832 and 1.1831 for the 17^3, 25^3 and 41^3 mesh, respectively. The difference between the results is less than 0.2%. For a more detailed look at the results, we present in Fig. 3 temperature, velocity and vorticity profiles for all three meshes. We observed only minor differences between solutions. The wall CPU time
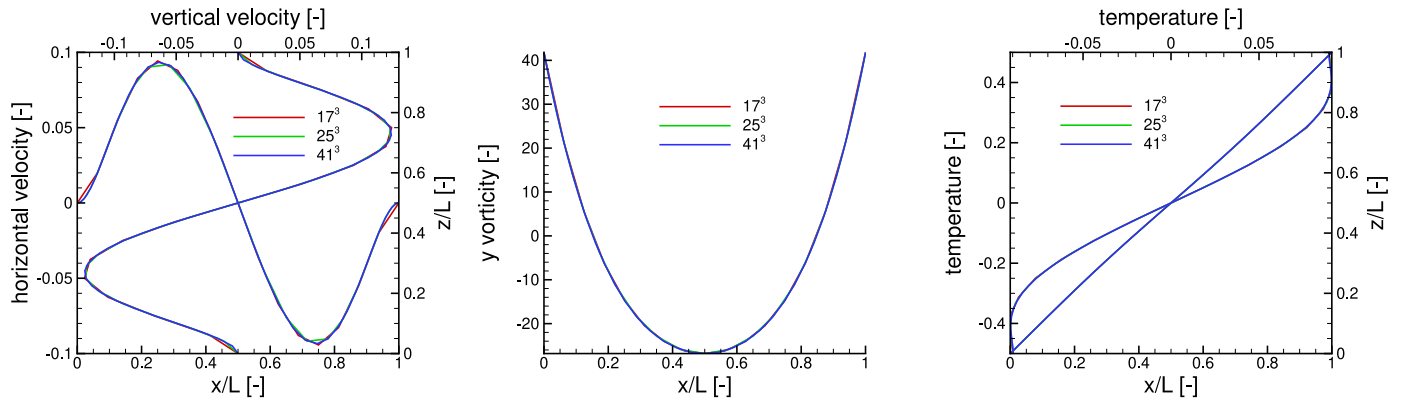
Fig. 3. Comparison of flow results on 17^3, 25^3 and 41^3 mesh for the $\varphi = 5\%$ and $Ra = 10^3$ case. Velocity (left panel), vorticity (middle panel) and temperature (right panel) are shown. Profiles were exported along the x and z axes through the centre of the domain.
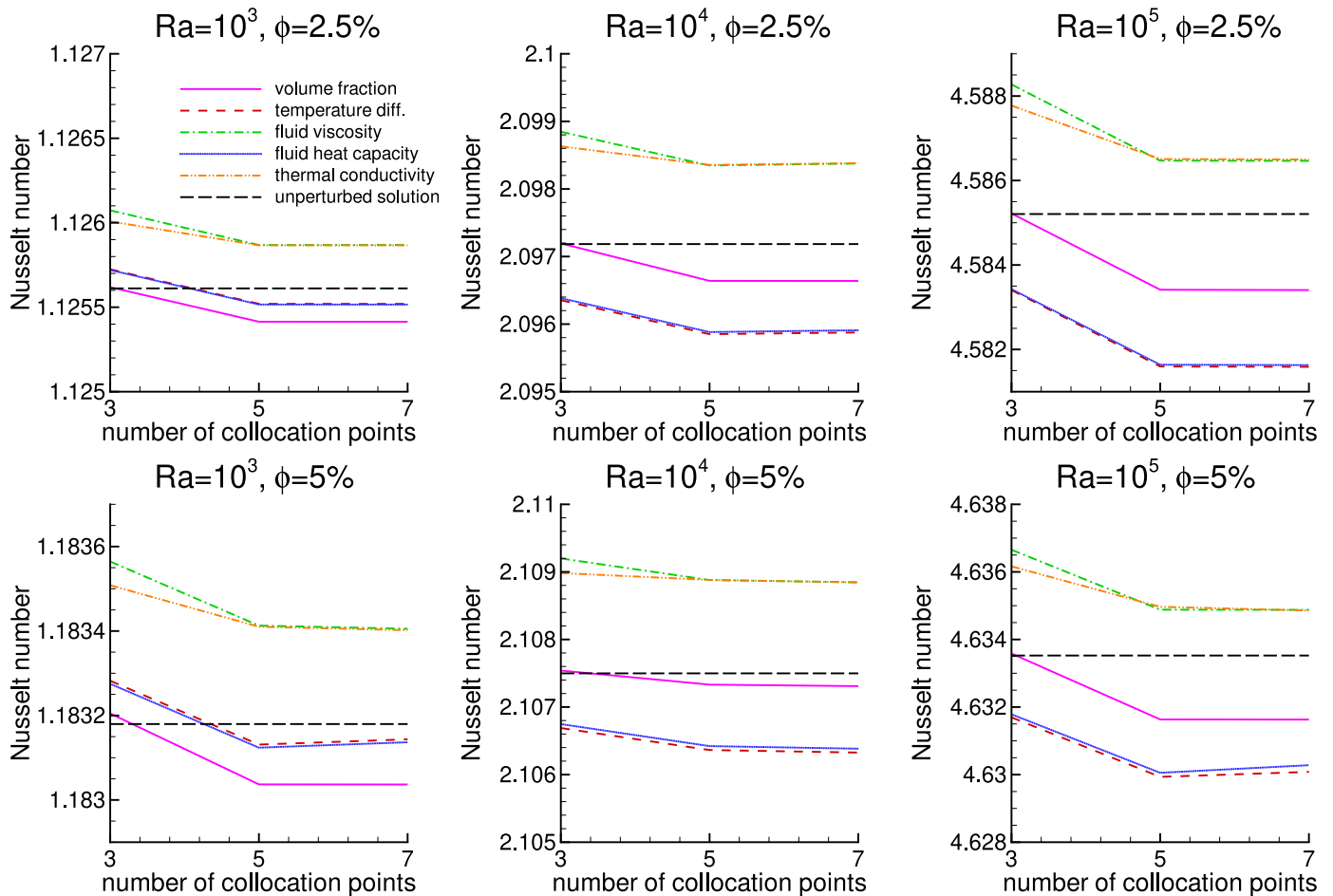

Fig. 4. Nusselt number results obtained for the six test cases using OAT analysis of all five random variables. Unperturbed solution is shown with black dashed line. The results obtained by using 5 and 7 collocation points are virtually identical.

needed for simulation was 1 min, 1 h and 12 h for the 17^3, 25^3 and 41^3 mesh, respectively, using Xeon E7 v3 Core i7. Based on this, we decided to perform all simulations using the 25^3 mesh. Using 16 processors, the total simulation time for all results in the paper was 3 months.

6. Results

In the first step, 12 input parameters were modelled as random, with uniform distribution set as 10% variation from nominal value: Volume

fraction, temperature difference, fluid viscosity, heat capacity, density, thermal conductivity, thermal expansion coefficient, characteristic dimension, particle heat capacity, density, thermal conductivity, thermal expansion coefficient. To reduce the dimensionality of the problem, 12 univariate Test Cases (TC) were done following the logic of the OAT principle. After comparing the variances from 12 TCs, five input variables are recognised as the important ones, while the others will be neglected in further computations. Those 5 input variables are: volume fraction, temperature difference, fluid viscosity, heat capacity, and thermal conductivity.
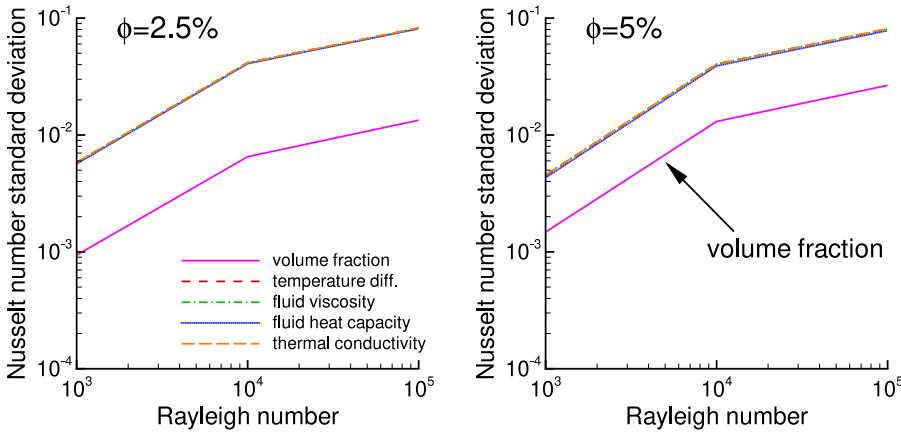
Fig. 5. Nusselt number standard deviation results obtained for the six test cases using OAT analysis with 7 collocation points of all five random variables. Volume fraction parameter shows significantly lower standard deviation, while all other random variables exhibit variance of similar order of magnitude.
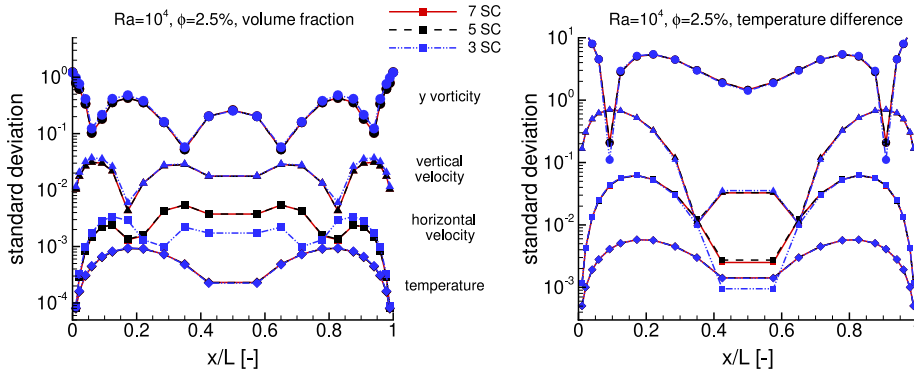

Fig. 6. Standard deviation profiles along the *x* axis through the centre of the domain. Standard deviation for main vortex perpendicular (*y*) component of vorticity, horizontal and vertical velocity and temperature are shown. OAT approach is used for volume fraction (left panel) and temperature difference (right panel) for the $Ra = 10^4$ and $\varphi = 2.5\%$ case.

6.1. OAT results

In Fig. 4 we examine the convergence of the stochastic analysis using the OAT approach. For each of the five random variables we performed OAT analysis using $m_k = 3$, 5 and 7 stochastic collocation points. We considered all six test cases. We observed that the results obtained by using 5 and 7 collocation points are virtually identical, and, thus, concluded that 5 collocation points are a good choice for the multi random variable analysis. For each of the six Test Cases this means that we need to run $5^5 = 3125$ simulations. Furthermore, the results of the OAT analysis show that the concentration seems to have the smallest impact on the results. Uncertainty in fluid viscosity and heat conductivity leads to an increase of the heat transport. In contrast, variation in thermal capacity and temperature difference leads to a decrease of heat transfer.

In Fig. 5 we observe an increase in the Nusselt number standard deviation with Rayleigh number value. This was expected, since at high Rayleigh number values, the temperature difference, which is driving the flow, is higher, and in consequence, convection becomes the most important heat transfer mechanism. Thus, the non-linear nature of the phenomenon is more pronounced, and so the results are more susceptible to changes in the input parameters. Comparing the random variables studied in the OAT analysis presented in Fig. 5, we observe that the standard deviation of volume fraction is significantly lower than the standard deviation of all other random variables. This is caused by the fact that the nanoparticle volume fractions used to prepare the nanofluids are small, and thus have a small influence of the effective properties of the nanofluid.

The Nusselt number is an integral parameter, showing the total heat transfer through the system. From an engineering point of view, it is important to note that the Nusselt number standard deviation is small, thus the overall heat transfer is not affected greatly by the changes in input parameters. For a more detailed look, we examined the result of the OAT analysis on the flow field profiles. In Fig. 6 we show standard deviations obtained by the OAT approach for the main vortex perpendicular (*y*) component of vorticity, horizontal and vertical velocity and temperature. Comparing standard deviations obtained using 3, 5 and 7 stochastic collocation points, we observe that the differences are small. Horizontal velocity displays a larger difference between the 3 SC points results and 5 and 7. Again, we conclude that a choice of 5 collocation points is reasonable.

6.2. Full tensor product results

In this subsection we present results obtained by considering five random variables and five stochastic collocation points for six cases (three Rayleigh numbers times two volume fractions). The mean temperature isotherms are shown in Fig. 7. In the case where conduction dominates heat transfer ($Ra = 10^3$), we observe an approximately linear change of temperature in the horizontal direction between the hot and the cold walls. On the other hand, when convection dominates ($Ra > 10^3$), we observe the appearance of temperature stratification, i.e. the top part of the domain is hot and the bottom cold, while there is an approximately linear distribution of temperature in vertical direction. At the same time, large temperature gradients appear close to the hot and cold walls.

Next, we focus on the $Ra = 10^5$, $\varphi = 2.5\%$ case and plot the standard deviation of temperature, velocity and vorticity in Fig. 8. The figure exposes clearly areas in the flow field where the greatest changes are expected. The largest temperature, velocity and vorticity changes are expected close to the hot and cold walls (or at the walls in the case of vorticity). This is due to the fact that the flow there exhibits the largest gradients of all field functions.

In the Figs. 9 and 10 we examine the areas in the flow where the highest changes are expected due to variation of the input parameters. We observe that, in the conduction dominated regime ($Ra = 10^3$), high
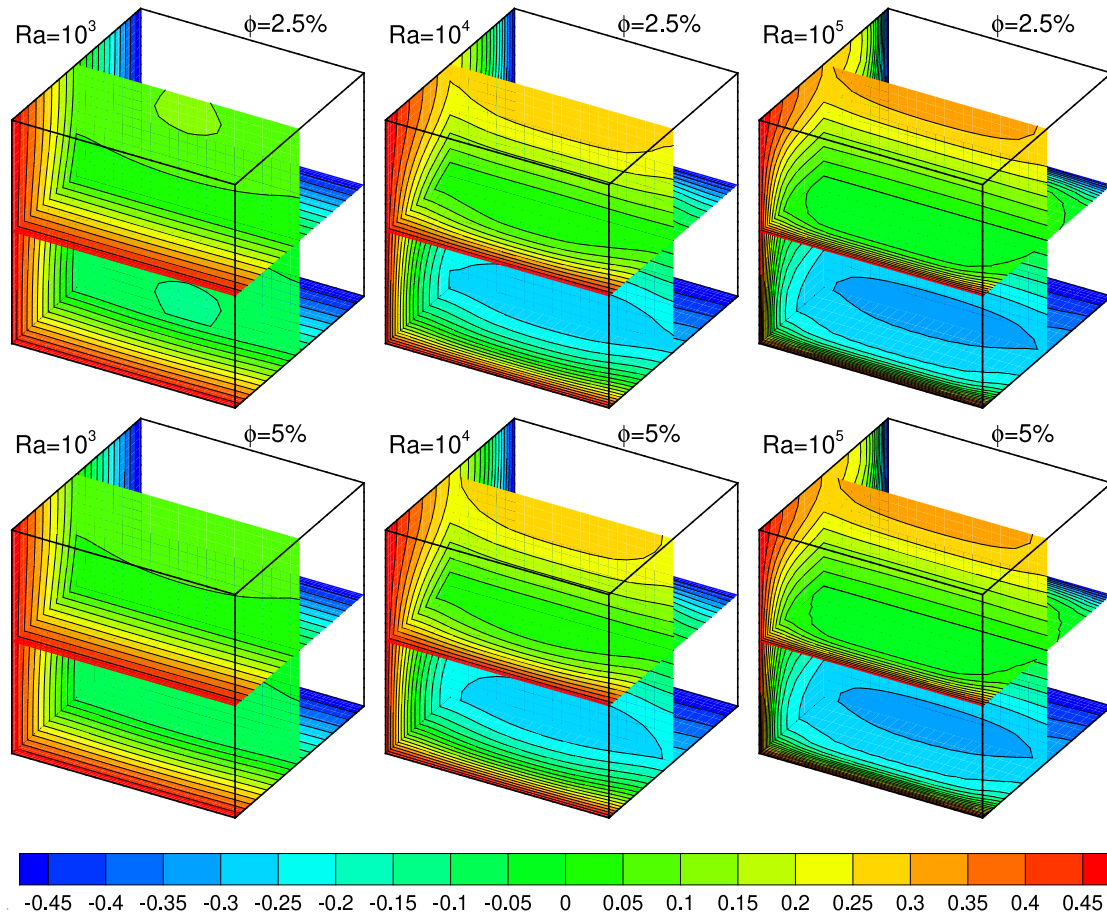
Fig. 7. Mean temperature isotherms shown on slices through the domain for all six test cases.

temperature field variance is observed close to the centre of the top and bottom walls. In the convection dominated regime ($Ra > 10^3$), the high variance areas are found closer to the bottom of the hot wall and the top of the cold wall. Looking at vorticity variance isosurfaces in Fig. 10, we also notice the area close to the vertical hot and cold walls to be the places where the vorticity variance is largest. Variance analysis has revealed that the areas with the largest flow solution uncertainty coincides with areas where the gradients on the flow fields are largest. In the present case, where we study natural convection between two differentially heated walls, this occurs near the vertical hot and cold walls.

From an engineering point of view, the most important parameter is the overall heat transfer through the cavity, which can be expressed as the Nusselt number. We present the relationship between overall heat transfer expressed as the Nusselt number and the temperature difference between the walls expressed as the Rayleigh number in Fig. 11. The increase of heat transfer with temperature difference is explained by the fact that convection is a more effective heat transfer mechanism than conduction. Thus, at high temperature differences, where convection dominates, the overall heat transfer is increased. The stochastic analysis showed that the variance of overall heat transfer also increases with the temperature difference. This is caused by the fact that flow and heat transfer are non-linear phenomena, and when the non-linear character is more important (as in the case of high temperature difference between the walls), small differences in input parameters have a larger influence on the results.

In Fig. 12, we observe the relationship between the y component vorticity flux through the vertical hot wall and the temperature difference between the walls. The vorticity flux increases with the

Table 2
Statistical moments for overall heat transfer expressed as Nusselt number.

Case		Nusselt number moments				
Ra	φ	Mean	Variance	Standard deviation	Skewness	Kurtosis
10^3	2.5%	1.126	$1.39 \cdot 10^{-4}$	$1.18 \cdot 10^{-2}$	0.319	2.86
10^4	2.5%	2.098	$69.4 \cdot 10^{-4}$	$8.33 \cdot 10^{-2}$	0.329	2.87
10^5	2.5%	4.586	$269 \cdot 10^{-4}$	$16.4 \cdot 10^{-2}$	0.312	2.85
10^3	5%	1.184	$0.86 \cdot 10^{-4}$	$0.93 \cdot 10^{-2}$	0.319	2.86
10^4	5%	2.109	$66.7 \cdot 10^{-4}$	$8.17 \cdot 10^{-2}$	0.334	2.88
10^5	5%	4.635	$265 \cdot 10^{-4}$	$16.3 \cdot 10^{-2}$	0.314	2.86

temperature difference. This is an indication of the intensity of the primary vortex, which is formed in the cavity. The primary vortex rotates the fluid mostly in the $x - z$ plane, thus the y component of vorticity is a measure of its strength. The stochastic analysis reveals that the influence of input parameters on the results is greater at a high Rayleigh number flows, where the temperature difference between the wall is higher, and the non-linear character of the phenomenon is more exposed.

In the Table 2 we present the statistical moments for overall heat transfer expressed as Nusselt numbers. We observe that the skewness and kurtosis seem to take constant values, irrespective of the Rayleigh number and nanoparticle concentration. Positive skewness is observed, meaning that a long tail of Nusselt number distributions can be observed on the right-hand-side of the distribution, where large Nusselt numbers lie. Kurtosis of less than 3 is observed, meaning that the Nusselt number distribution is platykurtic, i.e. broad.
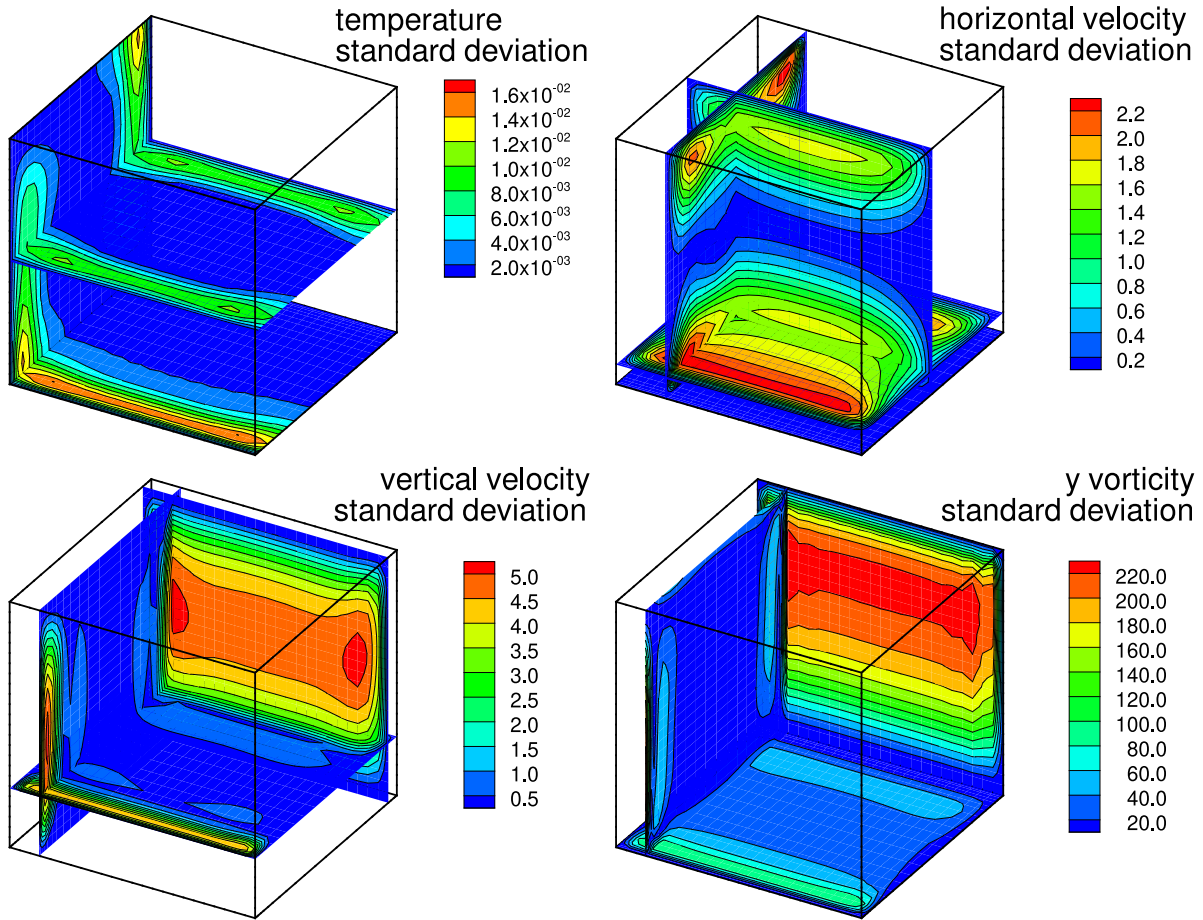
Fig. 8. Standard deviation of temperature, velocity and vorticity for the $Ra = 10^5$, $\varphi = 2.5\%$ case plotted in on slices through the domain. Areas where high values of standard deviation are observed are exposed.
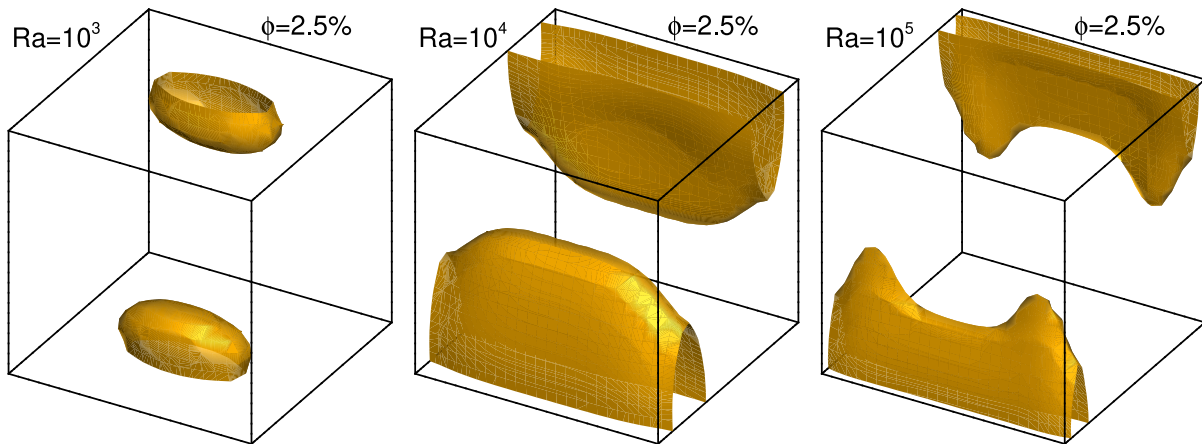

Fig. 9. Isofurfaces of temperature variance ($\sigma^2 = 10^{-4}$) reveals the areas in the flow field, where the temperature is most affected in changes in input parameters. Nanoparticle concentration $\varphi = 2.5\%$, Rayleigh number values are $Ra = 10^3$, $Ra = 10^4$ and $Ra = 10^5$ from left to right.

Skewness profiles are shown in Fig. 13. We observe values in the range of ± 0.5, which indicates that the skewness of flow field distributions changes within the domain. Changes are more evident in convection dominated flows (right panel in Fig. 13), where the skewness distribution appears chaotic. On the contrary, in conduction dominated flow, (left panel), we observe order, for example, the skewness is positive in areas of positive non-dimensional

temperature (on the warm side of the cavity) and negative on the other side.

Kurtosis of the temperature, velocity and vorticity fields is shown in Fig. 14. In most of the domain we observe a kurtosis of around 2.7, and, with that, platykurtic distribution of our flow fields. Isolated regions in the domain exist, where kurtosis is above 3, and the flow fields behave as leptokurtic.
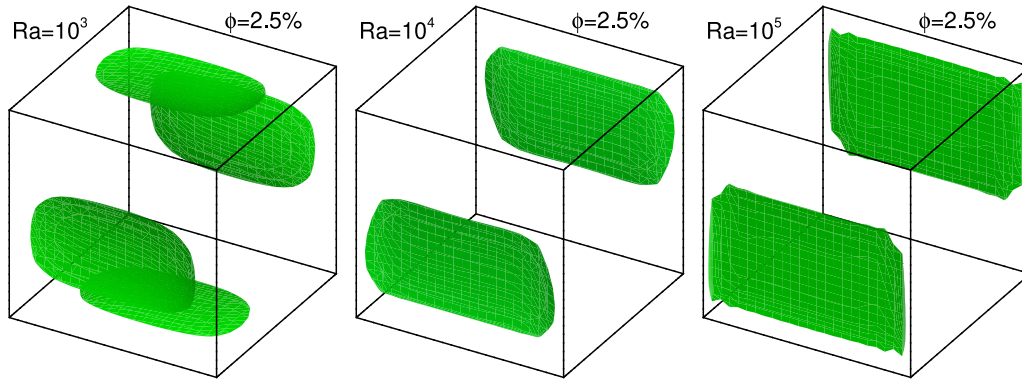
Fig. 10. Isofurfaces of y component of vorticity variance (set at one half of maximal value in the domain) reveals the areas in the flow field, where the vorticity is most affected in changes in input parameters. Nanoparticle concentration $\varphi = 2.5\%$, Rayleigh number values are $Ra = 10^3$, $Ra = 10^4$ and $Ra = 10^5$ from left to right.
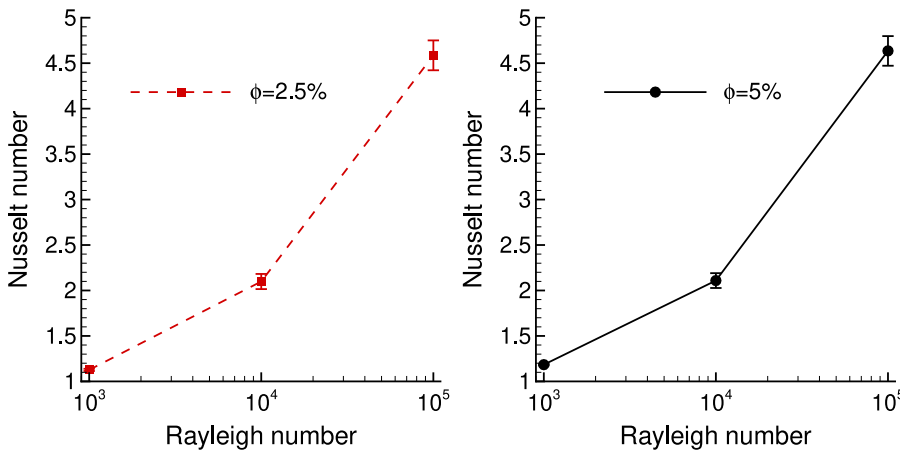

Fig. 11. Relationship between overall heat transfer expressed as the Nusselt number and the temperature difference between the walls expressed as Rayleigh number. Left panel shows the case of nanoparticle concentration $\varphi = 2.5\%$, right panel $\varphi = 5\%$. Standard deviation obtained by stochastic analysis is also displayed.
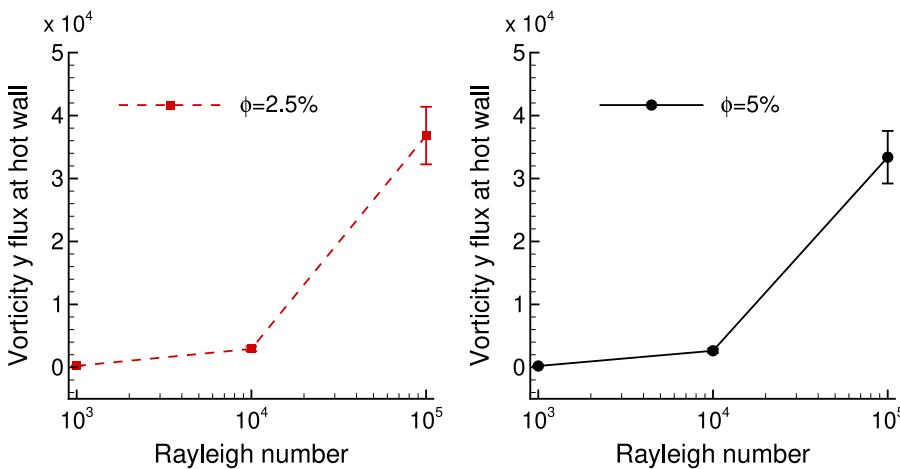

Fig. 12. Relationship between y vorticity component and the temperature difference between the walls expressed as Rayleigh number. Left panel shows the case of nanoparticle concentration $\varphi = 2.5\%$, right panel $\varphi = 5\%$. Standard deviation obtained by stochastic analysis is also displayed.
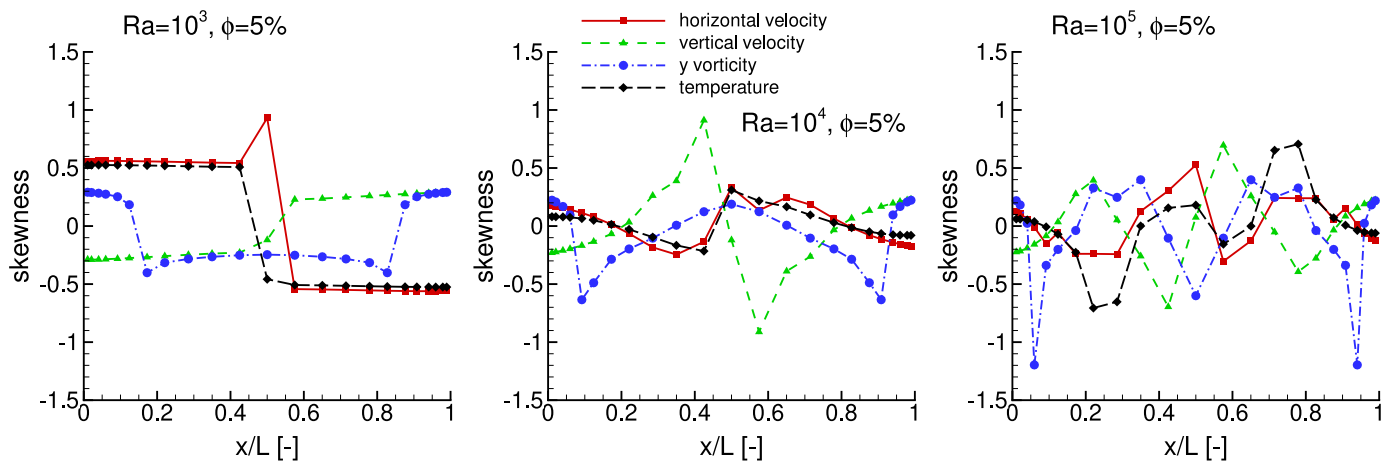
Fig. 13. Temperature, velocity and vorticity skewness profiles for $\varphi = 2.5\%$ and $Ra = 10^3$ (left panel), $Ra = 10^4$ (centre panel) and $Ra = 10^5$ (right panel).
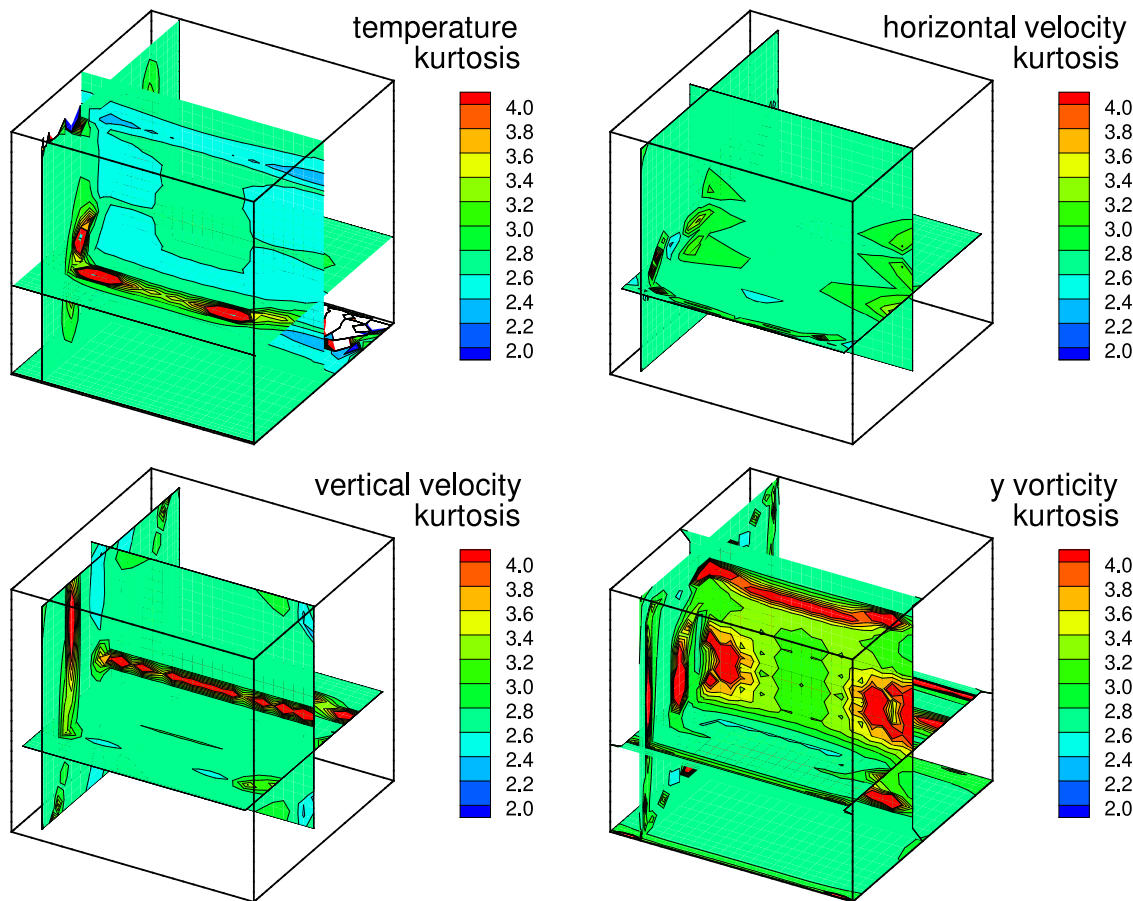

Fig. 14. Temperature, velocity and vorticity kurtosis for the $Ra = 10^5$, $\varphi = 2.5\%$ case plotted on slices through the domain. Areas where high or low values of kurtosis are observed are exposed.

7. Conclusions

We presented a Fast Boundary-Domain Integral Method for the simulation of natural convection of nanofluids, coupled with a Stochastic Collocation Method aimed at investigating the influence of input parameters on flow and heat transfer solutions. The results revealed that the influence of input parameters, such as nanoparticle volume fraction, heat conductivity, heat capacity, etc., is more important in convection dominated flows as opposed to conduction dominated flow regimes. Additionally, we discovered that the statistical moments reveal the greatest uncertainty in simulation results in areas, where large gradients of flow fields appear. In the case investigated in this paper, the area along the hot and cold walls exhibited the largest variance of simulation results. We found that fluid viscosity and nanoparticle thermal conductivity are the parameters which cause the largest variance in the simulation results. Care should be taken that the values of these parameters are as

accurate as possible when performing nanofluid simulations. The influence of other parameters, including the nanoparticle volume fraction, was smaller.

Acknowledgements

References

[1] Harish V, Kumar A. A review on modeling and simulation of building energy systems. Renew Sustain Energy Rev 2016;56:1272–92. doi:10.1016/j.rser.2015.12.040.

[2] Constantin P, Ciprian F. Navier–Stokes equations. Chickago University Press; 1998.

[3] Samadyar N, Mirzaee F. Numerical solution of two-dimensional weakly singular stochastic integral equations on non-rectangular domains via radial basis functions. Eng Anal Bound Elem 2019;101:27–36. doi:10.1016/J.ENGANABOUND.2018.12.008.

[4] Mirzaee F, Samadyar N. On the numerical solution of fractional stochastic integro-differential equations via meshless discrete collocation method based on radial basis functions. Eng Anal Bound Elem 2019;100:246–55. doi:10.1016/J.ENGANABOUND.2018.05.006.

[5] Wang G, Guo F. A stochastic boundary element method for piezoelectric problems. Eng Anal Bound Elem 2018;95:248–54. doi:10.1016/J.ENGANABOUND.2018.08.002.

[6] Hamdia KM, Ghasemi H, Zhuang X, Alajlan N, Rabczuk T. Sensitivity and uncertainty analysis for flexoelectric nanostructures. Comput Methods Appl Mech Eng 2018;337:95–109. doi:10.1016/j.cma.2018.03.016.

[7] Vu-Bac N, Lahmer T, Zhuang X, Nguyen-Thoi T, Rabczuk T. A software framework for probabilistic sensitivity analysis for computationally expensive models. Adv Eng Softw 2016;100:19–31. doi:10.1016/j.advengsoft.2016.06.005.

[8] Doubilet P, Begg CB, Weinstein MC, Braun P, McNeil BJ. Probabilistic sensitivity analysis using monte carlo simulation: a practical approach. Med Decis Mak 1985;5(2):157–77. doi:10.1177/0272989X8500500205. PMID: 3831638

[9] Xiu D, Karniadakis GE. Modeling uncertainty in flow simulations via generalized polynomial chaos. J Comput Phys 2003;187(1):137–67. doi:10.1016/S0021-9991(03)00092-5.

[10] Thapa M, Mulani SB, Walters RW. A new non-intrusive polynomial chaos using higher order sensitivities. Comput Methods Appl Mech Eng 2018;328:594–611. doi:10.1016/j.cma.2017.09.024.

[11] Mathelin L, Hussaini MY, Zang TA. Stochastic approaches to uncertainty quantification in CFD simulations. Numer Algor 2005;38(1):209–36. doi:10.1007/BF02810624.

[12] Xiu D, Hesthaven JS. High-order collocation methods for differential equations with random inputs. SIAM J Sci Comput 2005;27(3):1118–39. doi:10.1137/040615201.

[13] Constantine PG, Doostan A, Iaccarino G. A hybrid collocation/Galerkin scheme for convective heat transfer problems with stochastic boundary conditions. Numer Methods Eng 2009;80(6-7):868–80.

[14] Mathelin L, Hussaini MY. A Stochastic Collocation Algorithm for Uncertainty Analysis. Hanover: NASA Center for AeroSpace Information; 2003.

[15] Agarwal N, Aluru NR. Stochastic analysis of electrostatic MEMS subjected to parameter variations. J Microelectromech Syst 2009;18(6):1454–68.

[16] Bonnet P, Lallechere S, Chauviere C, Diouf F. Numerical simulation of a reverberation chamber with a stochastic collocation method. C R Phys 2009;10(1):54.

[17] Cheng X, Monebhurrun V. Application of different methods to quantify uncertainty in specific absorption rate calculation using a CAD-based mobile phone model. IEEE Trans Electromagn Compat 2017;59(1):14–23.

[18] Škerget L, Hribeřšek M, Kuhn G. Computational fluid dynamics by boundary domain integral method. Int J Numer Methods Eng 1999;46(8):1291–311. doi:10.1002/(SICI)1097-0207(19991120)46:8<1291::AID-NME755>3.0.CO;2-O.

[19] Liu Z, Wu F, Wang D. The multi-domain FMM-IBEM to model elastic wave scattering by three-dimensional inclusions in infinite domain. Eng Anal Bound Elem 2015;60:95–105. doi:10.1016/J.ENGANABOUND.2015.02.003.

[20] Ravnik J, Škerget L, Žunič Z. Fast single domain-subdomain BEM algorithm for 3D incompressible fluid flow and heat transfer. Int J Numer Methods Eng 2009a;77(12):1627–45. doi:10.1002/nme.2467.

[21] Wei X, Chen B, Chen S, Yin S. An ACA-SBM for some 2D steady-state heat conduction problems. Eng Anal Bound Elem 2016;71:101–11. doi:10.1016/J.ENGANABOUND.2016.07.012.

[22] Campos LS, de Albuquerque ÉL, Wrobel LC. An ACA accelerated isogeometric boundary element analysis of potential problems with non-uniform boundary conditions. Eng Anal Bound Elem 2017;80:108–15. doi:10.1016/J.ENGANABOUND.2017.04.004.

[23] Tibaut J, Škerget L, Ravnik J. Acceleration of a BEM based solution of the velocity–vorticity formulation of the Navier–Stokes equations by the cross approximation method. Eng Anal Bound Elem 2017;82:17–26. doi:10.1016/j.enganabound.2017.05.013.

[24] Tibaut J, Ravnik J. Fast boundary-domain integral method for heat transfer simulations. Eng Anal Bound Elem 2019;99:222–32. doi:10.1016/j.enganabound.2018.12.003.

[25] Ravnik J, Tibaut J. Fast boundary-domain integral method for unsteady convection–diffusion equation with variable diffusivity using the modified Helmholtz fundamental solution. Numer Algor2019;. doi:10.1007/s11075-019-00664-3.

[26] Ravnik J, Škerget L, Hribeřšek M. The wavelet transform for BEM computational fluid dynamics. Eng Anal Bound Elem 2004;28:1303–14.

[27] Xiao J, Wen L, Tausch J. On fast matrix vector multiplication in wavelet Galerkin BEM. Eng Anal Bound Elem 2009;33(2):159–67. doi:10.1016/J.ENGANABOUND.2008.05.006.

[28] Tanaka S, Sannomaru S, Imachi M, Hagihara S, Okazawa S, Okada H. Analysis of dynamic stress concentration problems employing spline-based wavelet Galerkin method. Eng Anal Bound Elem 2015;58:129–39. doi:10.1016/J.ENGANABOUND.2015.04.003.

[29] Yan F, Yu M, Lv J-H. Dual reciprocity boundary node method for convection–diffusion problems. Eng Anal Bound Elem 2017;80:230–6. doi:10.1016/J.ENGANABOUND.2017.05.001.

[30] Zhou F, You Y, Li G, Xie G, Li G. The precise integration method for semi-discretized equation in the dual reciprocity method to solve three-dimensional transient heat conduction problems. Eng Anal Bound Elem 2018;95:160–6. doi:10.1016/J.ENGANABOUND.2018.07.005.

[31] Peng H-F, Yang K, Cui M, Gao X-W. Radial integration boundary element method for solving two-dimensional unsteady convection–diffusion problem. Eng Anal Bound Elem 2019;102:39–50. doi:10.1016/J.ENGANABOUND.2019.01.019.

[32] AL-Bayati SA, Wrobel LC. Radial integration boundary element method for two-dimensional non-homogeneous convection–diffusion–reaction problems with variable source term. Eng Anal Bound Elem 2019;101:89–101. doi:10.1016/J.ENGANABOUND.2018.12.005.

[33] Ingber MS, Tanski JA, Alsing P. A domain decomposition tool for boundary element methods. Eng Anal Bound Elem 2007;31(11):890–6. doi:10.1016/J.ENGANABOUND.2007.03.002.

[34] Hsiao G, Khoromskij B, Wendland W. Preconditioning for boundary element methods in domain decomposition. Eng Anal Bound Elem 2001;25(4–5):323–38. doi:10.1016/S0955-7997(01)00029-7.

[35] Ramšak M. Multidomain BEM for laminar flow in complex fractal geometry. Eng Anal Bound Elem 2019;101:310–17. doi:10.1016/J.ENGANABOUND.2019.01.003.

[36] Choi S US. Enhancing thermal conductivity of fluids with nanoparticles. Dev Appl Non Newtonian Flows 1995;66:99–106.

[37] Mashali F, Languri EM, Davidson J, Kerns D, Johnson W, Nawaz K, et al. Thermophysical properties of diamond nanofluids: a review. Int J Heat Mass Transf 2019;129:1123–35. doi:10.1016/J.IJHEATMASSTRANSFER.2018.10.033.

[38] Moldoveanu GM, Minea AA. Specific heat experimental tests of simple and hybrid oxide-water nanofluids: proposing new correlation. J Mol Liq 2019;279:299–305. doi:10.1016/J.MOLLIQ.2019.01.137.

[39] Ramezanizadeh M, Alhuyi Nazari M, Ahmadi MH, Açskkalp E. Application of nanofluids in thermosyphons: a review. J Mol Liq 2018;272:395–402. doi:10.1016/J.MOLLIQ.2018.09.101.

[40] Mahian O, Kolsi L, Amani M, Estellé P, Ahmadi G, Kleinstreuer C, et al. Recent advances in modeling and simulation of nanofluid flows-Part I: Fundamentals and theory. Phys Rep 2019;790:1–48. doi:10.1016/J.PHYSREP.2018.11.004.

[41] Mahian O, Kolsi L, Amani M, Estellé P, Ahmadi G, Kleinstreuer C, et al. Recent advances in modeling and simulation of nanofluid flows-Part II: Applications. Phys Rep 2019;791:1–59. doi:10.1016/J.PHYSREP.2018.11.003.

[42] Minea AA, Estellé P. Numerical study on CNT nanofluids behavior in laminar pipe flow. J Mol Liq 2018;271:281–9. doi:10.1016/J.MOLLIQ.2018.08.161.

[43] Kaminski M, Ossowski RL. Prediction of the effective parameters of the nanofluids using the generalized stochastic perturbation method. Phys A Stat Mech Appl 2014;393:10–22. doi:10.1016/j.physa.2013.09.015.

[44] Ravnik J, Skerget L, Hribersek M. Analysis of three-dimensional natural convection of nanofluids by BEM. Eng Anal Bound Elem 2010;34(12):1018–30. doi:10.1016/j.enganabound.2010.06.019.

[45] Khanafer K, Vafai K, Lightstone M. Buoyancy-driven heat transfer enhancement in a two-dimensional enclosure utilizing nanofluids. Int J Heat Mass Transf 2003;46:3639–53.

[46] Brinkman HC. The viscosity of concentrated suspensions and solutions. J Chem Phys 1952;20:571–81.

[47] Maxwell JC. A treatise on electricity and magnetism. 2nd ed. Oxford, UK: Clarendon Press; 1881.

[48] Shukla RK, Dhir VK. Numerical study of the effective thermal conductivity of nanofluids. In: Proceedings of the 2005 ASME summer heat transfer conference; 2005.

[49] Wu JC, Thompson JF. Numerical solutions of time-dependent incompressible Navier–Stokes equations using an integro-differential formulation. Comput Fluids 1973;1:197–215.

[50] Šzkerget L, Hribešek M, Žunic Z. Natural convection flows in complex cavities by BEM. Int J Numer Methods Heat Fluid Flow 2003;13(6):720–35. doi:10.1108/09615530310498394.

[51] Hackbusch W. A Sparse matrix arithmetic based on H-matrices. Part I : Introduction to H-matrices. Computing 1999;108:89–108. doi:10.1007/s006070050015.

[52] Ramšak M, Škerget L. A subdomain boundary element method for high-Reynolds laminar flow using stream function-vorticity formulation. Int J Numer Methods Fluids 2004;46:815–47.

[53] Ravnik J, Skerget L, Zunic Z. Combined single domain and subdomain BEM for 3D laminar viscous flow. Eng Anal Bound Elem 2009b;33(3):420–4. doi:10.1016/j.enganabound.2008.06.006.

[54] Gunzburger M, Webster CG, Zhang G. An adaptive wavelet stochastic collocation method for irregular solutions of stochastic partial differential equations. Oak Ridge, Tennessee: Oak Ridge National Laboratory; 2012.

[55] Chauvire C, Hesthaven JS, Wilcox LC. Efficient computation of RCS from scatterers of uncertain shapes. IEEE Trans Antennas Propag 2008;55(5):1437–48.

[56] Saltelli A, Ratto M, Andres T, Campolongo F, Gatelli D, Saisana M, et al. Global sensitivity analysis: the primer. West Susex, England: John Wiley and sons, Ltd; 2008.

[57] Oztop HF, Abu-Nada E. Natural convection of water-based nanofluids in an inclined enclosure with a heat source. Int J Heat Fluid Flow 2008;29:1326–36.